Hillslope run-off thresholds with shrink-swell clay soils

Citation	Stewart R. D., Abou Najm M. R., Rupp D. E., Lane J. W., Uribe H. C., Arumí J. L. and Selker J. S. (2015). Hillslope run-off thresholds with shrink–swell clay soils. Hydrological Processes, 29(4), 557-571. doi:10.1002/hyp.10165
DOI	10.1002/hyp.10165
Publisher	John Wiley & Sons Ltd.
Version	Version of Record
Terms of Use	http://cdss.library.oregonstate.edu/sa-termsofuse

HYDROLOGICAL PROCESSES
Hydrol. Process. **29**, 557–571 (2015)
Published online 11 March 2014 in Wiley Online Library
(wileyonlinelibrary.com) DOI: 10.1002/hyp.10165

Hillslope run-off thresholds with shrink–swell clay soils

Ryan D. Stewart,[1,7]* Majdi R. Abou Najm,[2] David E. Rupp,[3] John W. Lane,[4] Hamil C. Uribe,[5] José Luis Arumí[6] and John S. Selker[7]

[1] *Crop and Soil Environmental Science Department, Virginia Polytechnic Institute and State University, Blacksburg, VA, USA*
[2] *Civil and Environmental Engineering, American University of Beirut, Beirut, Lebanon*
[3] *Oregon Climate Change Research Institute, College of Earth, Ocean, and Atmospheric Sciences, Oregon State University, Corvallis, OR, USA*
[4] *Branch of Geophysics, Office of Groundwater, US Geological Survey, Storrs, CT, USA*
[5] *Instituto Nacional de Investigaciones Agropecuarias, Quilamapu, Chile*
[6] *Departamento de Recursos Hidricos, Universidad de Concepción, Chillán, Chile*
[7] *Biological and Ecological Engineering Department, Oregon State University, Corvallis, OR, USA*

Abstract:

Irrigation experiments on 12 instrumented field plots were used to assess the impact of dynamic soil crack networks on infiltration and run-off. During applications of intensity similar to a heavy rainstorm, water was seen being preferentially delivered within the soil profile. However, run-off was not observed until soil water content of the profile reached field capacity, and the apertures of surface-connected cracks had closed >60%. Electrical resistivity measurements suggested that subsurface cracks persisted and enhanced lateral transport, even in wet conditions. Likewise, single-ring infiltration measurements taken before and after irrigation indicated that infiltration remained an important component of the water budget at high soil water content values, despite apparent surface sealing. Overall, although the wetting and sealing of the soil profile showed considerable complexity, an emergent property at the hillslope scale was observed: all of the plots demonstrated a strikingly similar threshold run-off response to the cumulative precipitation amount. Copyright © 2014 John Wiley & Sons, Ltd.

KEY WORDS hillslope; hydrology; vertisols; shrink–swell soils; run-off; infiltration

Received 9 August 2013; Accepted 27 January 2014

INTRODUCTION

Shrink–swell clay soils are found all over the globe, with up to 350 million ha being classified as either *vertisols* or *vertic* intergrades (Ahmad, 1996). Of that total, approximately 150 million ha can be classified as suitable for crops (Driessen *et al*., 2000), representing more than 5% of the world's total potential cropland (Buringh, 1989). *Vertic* soils are characterized by crack networks that form throughout the profile as the soil dries. When open, these crack networks exert substantial influence on hydrological processes. For example, cracks can act as preferential flow paths, channelling water and solutes around the soil matrix (Blake *et al*., 1973; Bouma and Dekker, 1978; Messing and Jarvis, 1990; Bronswijk *et al*., 1995; Greve *et al*., 2010) and increasing overall rates of infiltration (Jarvis, 1991; Heppell *et al*., 2000; Sanders *et al*., 2012) and evaporation (Weisbrod *et al*., 2009).

The presence, volume, and connectivity of crack networks influence when a soil will experience surface ponding and/or overland flow (run-off) (Wells *et al*., 2003). At a minimum, run-off should not propagate downhill until the cumulative volume of rainfall has exceeded the total crack volume (Kutílek, 1996). However, total crack volume can be difficult to measure or estimate as it often varies with soil water content (Jarvis and Leeds-Harrison, 1987; Morari and Knisel, 1997; Novák *et al*., 2002; Abou Najm *et al*., 2010).

Much of the research related to *vertic* soils has been focused on the shrinkage phase, when cracks are forming and increasing in volume. Numerous models have been developed to describe the soil shrinkage curve (Giráldez *et al*., 1983; McGarry and Malafant, 1987; Tariq and Durnford, 1993; Boivin *et al*., 2006) and to predict crack formation and propagation (Chertkov, 2002; Vogel *et al*., 2005). The corresponding swelling phase of *vertic* soils, in contrast, has received less attention, with only a few studies measuring or modelling the soil swelling curve (Peng and Horn, 2007; Chertkov, 2012). Likewise, few studies have documented observations of how cracks under rainfall actually seal during the swelling phase. Instead, it is assumed either that cracks seal from the

*Correspondence to: Ryan D. Stewart, Crop and Soil Environmental Science Department, Virginia Polytechnic Institute and State University, Blacksburg, VA, USA.
E-mail: ryan.stewart@vt.edu

bottom up (Bouma and Loveday, 1988; van Dam, 2000; Novák *et al*., 2002) or that the volume change in discrete crack layers is related to the amount of water that is adsorbed (Greco, 2002; Arnold *et al*., 2005). Some studies have called into question the assumption of the former (Favre *et al*., 1997; Römkens and Prasad, 2006; Greve *et al*., 2012), finding that cracks may initially seal at the soil surface, although consensus has not yet been attained because of the overall lack of observational data relating subsurface crack volume and soil water content.

If cracks do initially seal at the soil surface, the utility of surface-based crack measurements (Zein el Abedine and Robinson, 1971; Ringrose-Voase and Sanidad, 1996; Návar *et al*., 2002; Wells *et al*., 2003; Arnold *et al*., 2005; Abou Najm *et al*., 2010) may be limited. Instead, techniques that monitor subsurface crack dynamics, such as electrical resistivity tomography (ERT) (Samouëlian *et al*., 2003; Samouëlian *et al*., 2004; Amidu and Dunbar, 2007; Sentenac and Zielinski, 2009; Greve *et al*., 2010; Greve *et al*., 2012), or physically installing subsurface monitoring instruments into representative cracks (Stewart *et al*., 2012) may prove more informative about the rate and degree to which cracks close.

To date, however, few studies have focused on the relationship between moisture content and crack dimensions both at and below the soil surface. Moreover, none has successfully integrated measurements of soil water content and crack closure to measurements of hydrological processes such as infiltration and overland flow. This present study, therefore, had three main objectives: (1) to observe and quantify how water moves through an initially dry *vertic* soil under irrigation at rates and amounts similar to a heavy rainstorm; (2) to monitor soil properties and parameters such as soil water content, effective hydraulic conductivity, and relative crack volumes and surface areas as the soil profile went from dry to wet conditions; and (3) to identify threshold points associated with run-off beginning and then becoming the dominant hydrological response.

MATERIALS AND METHODS

Site location

The study took place in the *Secano Interior* region of south-central Chile, which is located on the leeward (eastern) side of the Chilean coast range. The climate of the *Secano Interior* is semi-arid with an annual mean precipitation of 0.7 m; the majority of precipitation occurs in the months of May–August, based on a government-maintained weather station located in San Agustín de Puñual (36°23′47.53″S, 72°25′45.25″W), located 7 km from the study area.

The field site was located near the commune of Ninhue (36°25′04″S, 72°31′05″W) (Figure 1), on a hillside of moderate slope. The site was covered by a native pasture with a few scattered pines (*Pinus radiata*) and acacia (*Acacia caven*) trees. By January (i.e. midsummer) of each year, the plant available water became depleted, causing the grasses to senesce. Thus, transpiration by the grasses was assumed to be insignificant during midsummer and late summer. The site's soils were developed from a granitic source rock, with a depth to saprolite varying from approximately 0.6 to 0.8 m. Hydrometer and X-ray diffraction analyses were performed on samples taken from the surface down to 0.85 m. Sand, silt, and clay percentages and the clay fraction mineralogy are summarized in Table I.

Two sets of nine 3.5 × 11-m instrumented run-off plots were located on the hillside (Figure 2). The upper set (plots U1–U9) was located on the hillslope shoulder (12° average slope). The lower set (plots L1–L9) was located on the backslope (18.5° average slope). Each set of plots was further divided into groups of three, with an intragroup spacing of 1 m and an intergroup spacing of 1.5 m. Along the perimeter of each plot, except for the downhill edges, a 0.3-m tall plastic divider was embedded into the soil to a depth of 0.15 m.

Run-off collection

At the downhill edge of each plot, a covered concrete floor and channel collected all overland flow. Once in the channel, the flow was directed to a single 4 × 0.09-m PVC pipe and conveyed to the run-off measurement systems.

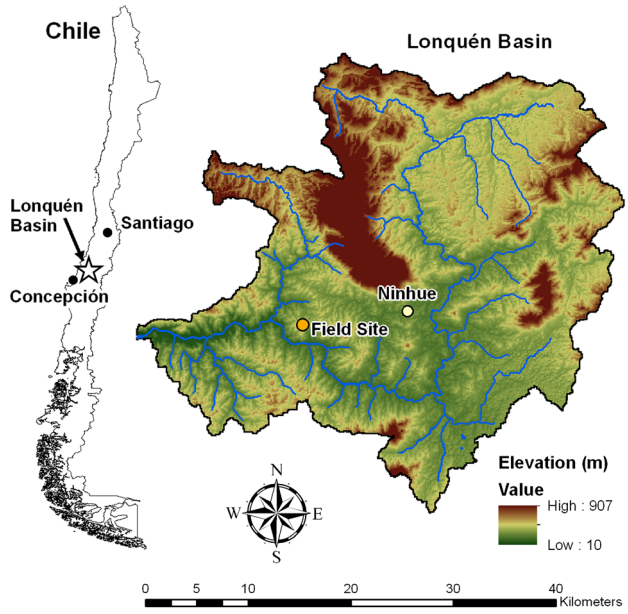

Figure 1. Map showing relative position within Chile of the Lonquén Basin and the location of the field site within the basin

Table I. Percentages of sand, silt, and clay and mineralogical momposition of the clay (<2 μm) fraction

Depth (cm)	No. of samples		Particle size distribution (%)			Texture	Mineral % in the <2 μm fraction			
	PSD	XRD	Sand	Silt	Clay		Smectite	Vermiculite	Kaolinite	Illite
5	15	1	52 ± 11	33 ± 12	15 ± 8	Loam	15	10	70	5
10	13	2	51 ± 14	32 ± 15	18 ± 12	Loam	20	5	70	5
20	10	1	29 ± 6	29 ± 4	42 ± 7	Clay	45	10	40	5
30	9	2	23 ± 6	31 ± 7	46 ± 12	Clay	30	20	45	5
60	5	2	23 ± 6	27 ± 5	50 ± 2	Clay	30	15	50	5
85	3	2	48 ± 6	31 ± 5	21 ± 11	Loam	50	10	35	5

PSD = particle-size distribution. XRD = X-ray diffraction.

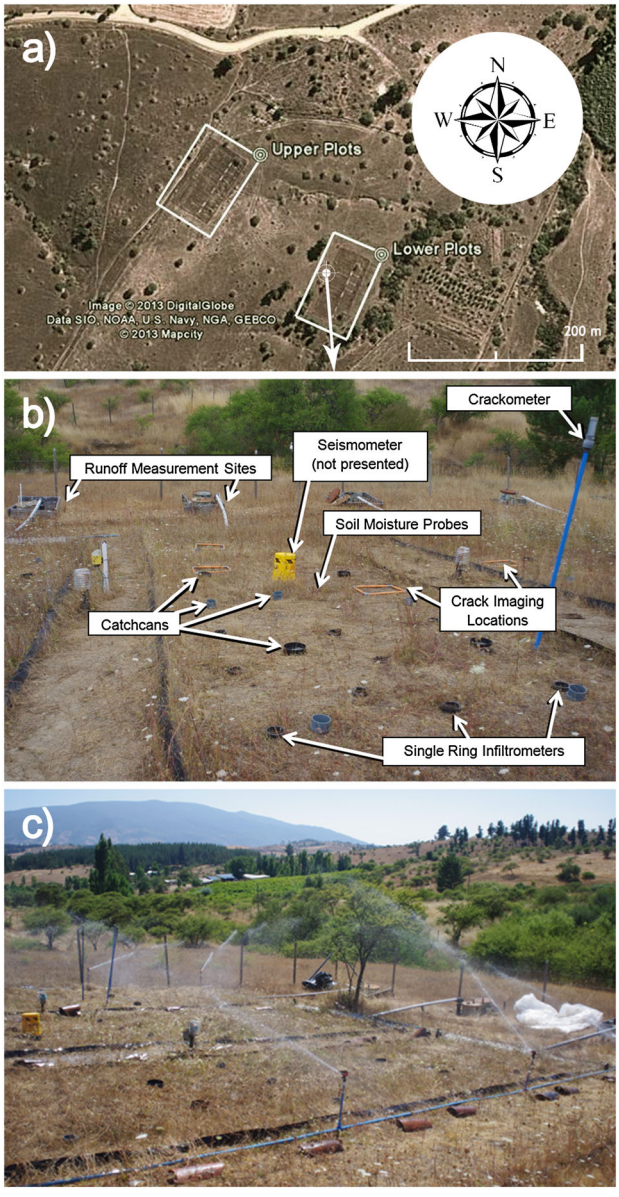

Figure 2. (a) Overhead view of the field site, with the two sets of run-off plots highlighted, (b) plot L5, with examples of notable equipment and instruments highlighted, and (c) plots L1–L3, showing how the configuration of the irrigation system divided the plots into sets of three

In 2011 (year 1 of the experiment), all run-offs were collected and measured in twin 0.2-m^3 metal barrels. The two barrels were connected via a narrow chute near the top, with the chute accepting the water from one of ten equal-sized slots, so that when the water level reached the chute, approximately 10% of the incoming water was transported to the second barrel. The remaining 90% of the water was spilled into a 6-m long buried drain pipe that conveyed the overflow downhill from the site. Each barrel system was located 4 m downhill from the irrigation plots in a 1-m deep pit with a cement slab and wooden slats to support the sides. The barrels were periodically emptied using either a hand pump or a bucket.

In 2012 (year 2 of the experiment), the run-off monitoring system in plots L2–L5 and plots U2–U4 and U6 was improved because of shortcomings in the two-barrel system such as the high noise-to-signal ratio in the second (1:10 reduction) barrel and the need to frequently empty the barrels during the irrigation experiments. In the improved 'leaky bucket' system, run-off was directed into a vertical 0.1-m pipe capped at the bottom end. The 0.1-m pipe was perforated with holes of increasing diameter with height. After passing through a screen to filter debris, the run-off entered the pipe and drained from the holes. Water level within the pipe was measured using a HOBO U20-002 pressure transducer (Onset Corporation), set to record at 15-s intervals. Based on the hole configuration and the water level within the pipe, pipe discharge rate q was inferred using Torricelli's law:

$$q = \sum_{i=1}^{n} c_i A_i \sqrt{2gH_i} \tag{1}$$

where H is the height of water (relative to hole i), g is the gravitational constant, A is the cross-sectional area of hole i, c is a correction term that accounts for roughness of hole i (with $c = 1$ representing a smooth hole), and n is the number of holes below the water level. A laboratory calibration found c to equal 0.96. Run-off rate was then calculated as q plus the rate of change in water stored in the pipe, dV/dt, where V is the volume of water stored in the pipe.

Soil water content

To measure soil water content, the midpoint of each plot was instrumented with Decagon Devices 5TM capacitance probes at depths of 0.15, 0.30, 0.60, and 0.85 m. Measurements began on 25 May 2010, with a frequency of 15 min that was increased to every minute during active experimentation periods. To correct for minor temperature effects on the 5TM soil moisture probe readings, a first-order correction was applied to the 0.15- and 0.30-m probes, as recommended by Campbell (2001).

$$\theta_t = \left[\frac{T_r + \beta}{T_i + \beta}\right]\theta_m \tag{2}$$

where θ_t is the temperature-corrected water content, θ_m is the measured water content, T_i is the temperature of the reading, T_r is the temperature of the probe calibration, and β is a constant.

Surface-connected cracks

Representative surface-connected cracks were chosen within the plots for monitoring. Monitoring consisted of two approaches: (1) large cracks within three plots were instrumented with the *crackometer* instrument (Stewart *et al.*, 2012), which consisted of a 1-L intravenous therapy bag placed within the crack that was then filled with water from a connected standpipe, enabling measurement of relative volume change over the sampled area and (2) medium-to-large sized cracks from within five plots were marked by 0.5 × 0.5-m frames and then imaged throughout the experiment from a height of 0.6 m using a Pentax K-x digital SLR and a 28-mm lens. The surface area of the cracks was quantified by converting the image to black and white, representing the crack and soil, respectively, and then counting the number of black pixels. Minor colour and contrast adjustments were made on some images to eliminate artefacts such as shadows, cables, and vegetation.

Irrigation experimental setup

An irrigation system was used to provide controlled water application to the plots. The system was constructed from a 0.032-m PVC pipe, laid out in a 12 × 12-m square, which enabled the simulator to be placed around a group of three run-off plots. The two sides of the simulator parallel to the slope direction each had four sprinkler heads, with one at each corner and two spaced equally in between. Each sprinkler head could be adjusted for length of travel as well as angle and intensity of the water stream. This allowed for on-the-fly adjustments of individual sprinkler head in an attempt to create uniform coverage.

The rainfall simulator was used for 2-week periods in January of both 2011 and 2012, when the antecedent dry conditions had created large crack networks throughout the soil plots. Water for the irrigation system was extracted from the *Río Lonquén* (36°27′29.891″S, −72°21′5.461″W, approximately 18 km from the site by road) by a water truck, and was pumped either directly from the truck or from a temporary storage tank constructed adjacent to the plots. Each irrigation event was therefore equal to the capacity of the water truck, or approximately 10 m^3 of water. This volume corresponded to a rainfall rate of between 0.3 and 0.8 mm min^{-1} (20–50 mm hr^{-1}) or a per event depth of irrigation that ranged from 20 to 60 mm.

As a result of time and water limitations, only 9 of the 18 plots were irrigated in year 1, and only 12 of 18 were irrigated in year 2. For both years, the irrigated plots were grouped into sets of three (L1–L3, L4–L6, U1–U3, and U4–U6). During year 2, each set was assigned a different experimental treatment, where the irrigation rate and intervals were varied (irrigation schedules for both years are shown in Table II). The application rates were designated as high (50–120 mm d^{-1}, with a mean value of 85 ± 20 mm d^{-1}), mixed (20–160 mm d^{-1}, with a mean value of 75 ± 50 mm d^{-1}), and low (20–60 mm d^{-1}, with a mean value of 45 ± 10 mm d^{-1}). The treatments also

Table II. Irrigation schedule for 2011 and 2012

Year 1 (2011)										
Date	1/5	1/6	1/7–1/10	1/11	1/12	1/13–1/16	1/17	1/18		
Day	1	2	3–6	7	8	9–12	13	14		
L1–L3							1[a] 2[a]	3[a] 4[a]		
L4–L6				1	2 3 4		5	6[b]		
U1–U3	1 2	3 4		5						
Year 2 (2012)										
Date	1/11	1/12–1/16	1/17	1/18	1/19	1/20–1/22	1/23	1/24	1/25	1/26
Day	1	2–6	7	8	9	10–12	13	14	15	16
L1–L3	1 2		3 4					5 6		
L4–L6				1	2 3 4		5			
U1–U3			1					2		3 4 5
U4–U6			1	2				3	4	5

For the 2012 data, the gray shading indicates periods where the plots were covered with plastic to prevent evaporation.
[a]First ERT monitoring event.
[b]Second ERT monitoring event.

varied in the intervals between irrigation, with multiday intervals considered long time and subday intervals considered short time.

Plots L1–L3 were irrigated with the long-time high-rate (LT-HR) treatment, in which two truckloads were applied on days 1, 7, and 14, and in between the plots were covered with a 0.2-mm plastic to inhibit evaporation. Plots L4–L6 were irrigated with the short-time mixed-rate (ST-MR) treatment, in which four truckloads of water were applied over days 8 and 9, with a fifth truckload applied on day 13. Plots U1–U3 were irrigated with a long-time mixed-rate (LT-MR) treatment, in which one truckload was applied at days 7 and 14, and three loads were applied on day 16. Plots U4–U6 were irrigated with a long-time low-rate (LT-LR) treatment, in which one truckload was applied on days 7, 8, 14, 15, and 16, and in between irrigations, the plots were covered with the 0.2-mm plastic. Differences in the experimental treatments were analysed by comparing the cumulative amount of run-off after 23 cm of irrigation water had been applied.

During irrigation events, water application was recorded by catch cans located within the plots. Each plot had 11 catch cans, placed in a regular pattern. The uniformity of irrigation within each plot was analysed using the distribution uniformity (DU) coefficient, which can be described as (Warrick, 1983)

$$DU = 1 - \frac{\text{average of the lowest quartile of depth of water infiltrated}}{\text{average depth of water infiltrated}} \quad (3)$$

In order to derive rainfall–run-off relationships, per-event amounts of precipitation were calculated based on the mean amount of water collected in the catch cans for each plot.

Monitoring of soil properties

In 2012, single-ring infiltration measurements were made in plots L2, L5, U2, and U5 throughout the course of the rainfall infiltration experiment. Each test consisted of 9–13 single rings of 0.096-m diameter, shallowly installed in a 2 × 2-m grid. Care was taken to ensure that rings were installed in locations without visible shrinkage cracks so that infiltration would occur through the soil peds rather than through large macropores. Along with each single ring test, soil cores (volume = 6.87×10^{-3} m^3) from each of these plots were collected for quantification of gravimetric water content and bulk density.

Infiltration (I) as an equivalent water depth was modelled using the Philip's equation for one-dimensional vertical infiltration (Philip, 1957):

$$I = S\sqrt{t} + At \quad (4)$$

where S is the soil sorptivity, and A is term to describe the flow's resistance to gravity. For the purposes of this study, it was assumed that three-dimensional infiltration effects could be approximated by assuming that the effective hydraulic conductivity (K_{eff}) was equal to A/0.55 (Stewart, 2013).

Additionally, during the 2011 experiment, several other infiltration methods were used on the site during dry conditions ($\Theta_0 < 0.3$). Those methods included Guelph Permeameter measurements taken at 0.25-m depth and double-ring infiltrometer and Mini-disk Tension Permeameter measurements taken at the soil surface. The Guelph Permeameter (Soilmoisture, Inc., Guelph 2800K1) was installed, operated, and analysed using Equations (19) and (22) from Verbist *et al*. (2013). The double-ring infiltrometer consisted of an outer ring of 0.60 m and an inner ring of 0.30 m, installed to a depth of approximately 0.1 m. Measurements were analysed using Equation (3.28) from Selker *et al*. (1999). The Mini-disk Tension Permeameter (Decagon Devices, Inc.) was operated and analysed according to the manufacturer's recommendations. The applied tension was approximately −0.01 m, and the soil was assumed to be a clay loam based on the particle size distribution of samples taken in the upper 0.2 m of soil (Table I).

Geophysical monitoring

During the irrigation experiments, it was observed that water seeped through the walls of the collection barrel pit at many of the experimental plots, often beginning concurrently with the initiation of surface run-off. Because the entirety of the surface run-off was being conveyed into the barrels, the source of this seepage water must have been lateral subsurface flow. An experiment using direct-current resistivity was therefore conducted during the 2011 irrigations to determine at what point during water application these subsurface lateral pathways became active and how long they retained water. A four-electrode Wenner array with an A-spacing of 2 m was installed 3 m downslope of the lower edge of an irrigation plot, with the array oriented perpendicular to the hillslope and expected direction of flow (Figure 3). The direct current resistivity method was used to measure resistance and calculate apparent resistivity using a Sting R1 earth resistivity meter (Advanced Geosciences, Inc. instruments). Apparent

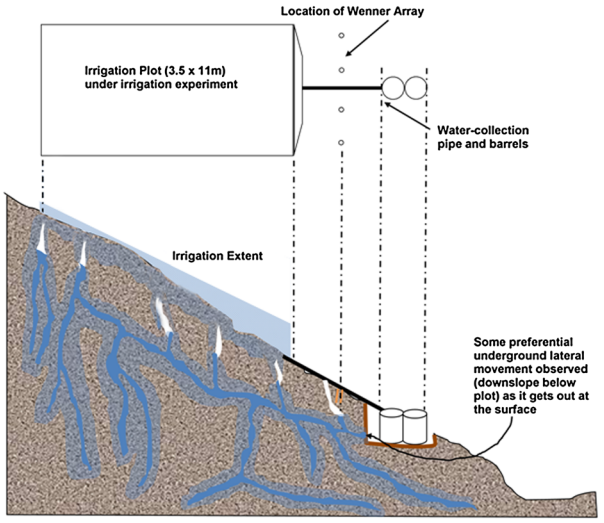

Figure 3. Schematic of an experimental field plot and conceptualisation of water distribution in the hillslope crack system in response to the irrigation. In 2011 (year 1), two of the plots were outfitted with Wenner arrays of electrodes to measure the existence of subsurface preferential flow paths

resistivity measurements were then used to calculate the change in apparent electric conductivity ($\Delta\sigma$) by

$$\Delta\sigma = (\Omega_i - \Omega_0)^{-1} \quad (5)$$

where Ω_i is the apparent resistivity measured through time, and Ω_0 is the initial apparent resistivity.

Two separate monitoring events were conducted. In the first event (which corresponded to year 1, irrigations 1–4 in plot L2), the soil was initially dry. In the second monitoring event (which corresponded to year 1, irrigation 6 in plot L5), the soil was already wetted from previous simulated rainfall applications. These two monitoring events are indicated on the irrigation schedule of Table II. Electrical conductivity of the irrigation water, as measured from samples collected throughout the experiment, was 0.31 ± 0.01 mS cm^{-1}.

RESULTS

Distribution of applied water

The cumulative amounts of applied water and the DU coefficients varied greatly between plots (Table III), but in general, both were highest for the plots furthest to the north-east (i.e. L1, L4, U1, and U3) and lowest for the plots furthest to the south-west of each group (i.e. L3, L6, U3, and U6). This pattern was mostly the result of the prevailing wind pattern from the south-west to the north-east during the experiments despite measures taken to shield the fields from wind by installing 2-m high and 20-m long plastic windbreaks on the upwind side of plots.

Table III. Cumulative irrigation amounts and the distributed uniformity (DU) coefficient for both years of the experiment

	Cumulative irrigation (cm)		DU coefficient	
Plot	Year 1[a]	Year 2	Year 1	Year 2
L1	17.4	35.5	0.75	0.81
L2	15.2	27.2	0.72	0.76
L3	15.6	24.1	0.69	0.48
L4	26.1	24.5	0.73	0.66
L5	22.4	24.1	0.74	0.77
L6	22.1	23.2	0.7	0.48
U1	16.8	25.7	0.67	0.76
U2	12.0	24.4	0.61	0.72
U3	14.2	24.1	0.64	0.66
U4	N/A	27.3	N/A	0.79
U5	N/A	23.3	N/A	0.76
U6	N/A	23.1	N/A	0.50

[a] An additional 2.1 cm of natural precipitation occurred during the study period.

Soil water content

The soil water content response to the irrigation showed several interesting characteristics. For one, the water did not appear to progress through the soil profile as a classic wetting front. While some of the profiles appeared to wet from the top down, others showed the opposite behaviour (Figure 4). Adjacent plots U2 and U3 showed this contrast most vividly (Figure 4). In the former, the soil wetted from top to bottom. In the latter, however, the soil water content first increased at the 0.85-m depth, then at the 0.60-m depth, while the upper probes in the profile did not substantially increase in moisture until after the lower depths had reached their maximum values. Looking at plot L2, it can be seen that the 0.60-m probe responded to the increase in moisture before any other probe, followed soon thereafter by the 0.15-m probe. Those two probes then responded in unison, showing an increase in volumetric water content of more than 10% over the first two irrigation events, whereas the 0.30- and 0.85-m probe readings did not change over that same period. In the third irrigation event, the 0.30-m probe showed increased soil water content, while the 0.85-m probe did not respond until the fourth irrigation.

These data indicate the ability of shrinkage cracks to preferentially provide moisture to various depths and locations within the soil profile. This, in turn, suggests that the wetting of *vertic* soils is a three-dimensional process, with infiltration occurring at ped-crack interface in addition to wetting from the top (and possibly the bottom) of the profile. The amount, rate, and depth of wetting showed major heterogeneity, beyond that predicted by three-dimensional crack-based wetting models (Hoogmoed and Bouma, 1980). While heterogeneous wetting would seem to argue for inclusion of a soil water

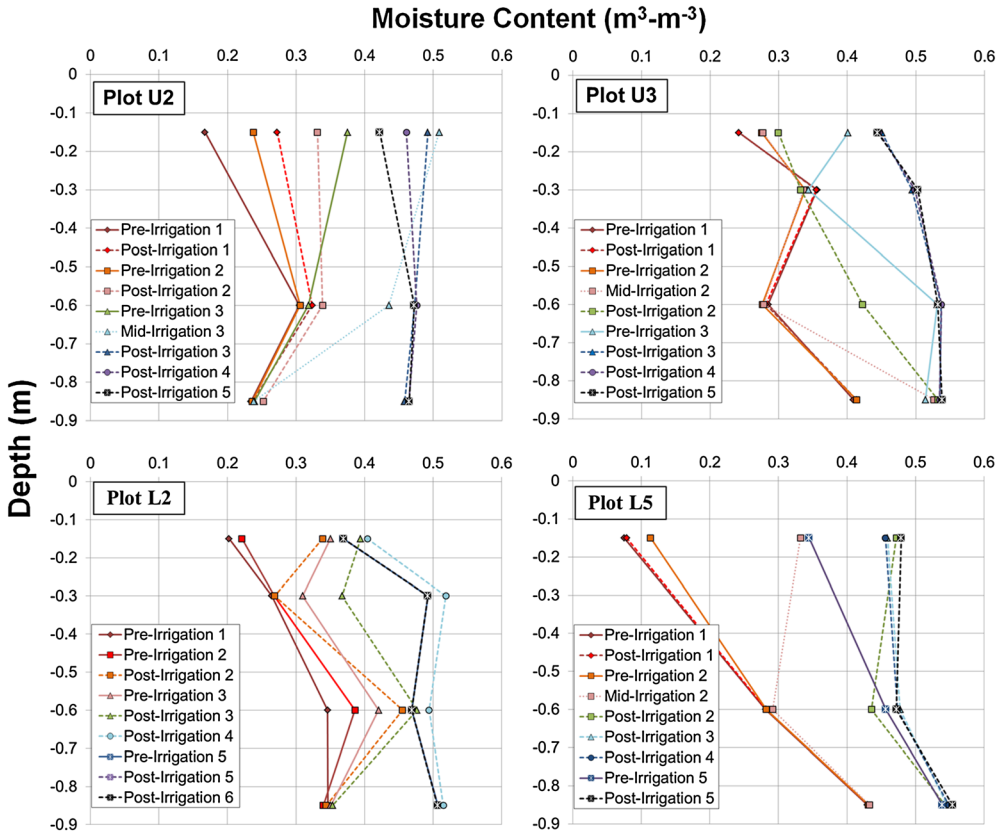

Figure 4. Wetting profile for plots U2, U3, L2, and L5 during the 2012 (year 2) irrigation experiment. Solid lines indicate pre-irrigation readings, dotted lines indicate mid-irrigation readings, and dashed lines indicate post-irrigation readings

content distribution term into models that predict infiltration and by extension run-off rates based on moisture content of the soil profile (Smith and Goodrich, 2000; Chen and Young, 2006; Brocca *et al*., 2008), studies on non-cracking soils indicate that initial horizontal soil water content distribution is an unimportant term when considering run-off generation at medium and large scales (Goodrich *et al*., 1994; Morbidelli *et al*., 2012).

When run-off ratio (run-off divided by rainfall) was plotted as a function of soil water content, the system showed a near-binary threshold (Figure 5), which may best be described as 'hockey-stick shaped' (Ali *et al*., 2013). While the shape of this threshold was similar to those observed for rigid (non-swelling) soils (James and Roulet, 2009; Penna *et al*., 2011), it stands in contrast to the 'sigmoid'-shaped threshold seen by Zehe *et al*. (2007) for a cracking clay soil. However, Zehe *et al*. (2007) determined run-off ratio using stream measurements and estimated soil water content using modelled data; thus, their results are not considered to be directly comparable.

The capacitance sensors used in this study were small, with a limited sampling volume (~3×10^{-4} m^3). Therefore, the observed near-binary run-off response may have been caused by the limited ability of these small-scale capacitance sensors to measure soil water content in *vertic* soils (Dinka and Lascano, 2012). It is possible that larger sensors such as time-domain reflectometer (te Brake *et al*., 2012) or alternate methods such as neutron attention measurements (which can measure volumes of ~1–4 m^3) (Evett *et al*., 2009) would be able to measure both outer and inner ped soil water content and therefore reveal the true effect of soil water content on run-off.

Crack volumes and dynamics

The *crackometer* data suggest that the amount of crack closure may be temporally decoupled from point measurements of soil water content (Figure 6). For example, the data from *crackometer* U3-1 showed the soil profile approaching field capacity water content (considered to be the maximum stable water content as measured by the soil water content probes) before the monitored crack began to seal. *Crackometer* L4-4 showed the opposite response, in that the crack was nearly sealed before the lower soil profile even started to wet. *Crackometer* L1-4 showed an intermediate behaviour.

Imaging analysis suggests that the surface cracks had a more uniform response to changes in near-surface soil water content (Figure 7). In the initial stages of wetting, soil water content (at 0.15-m depth) increases of around 10% caused the surface cracks to close to less than 40%

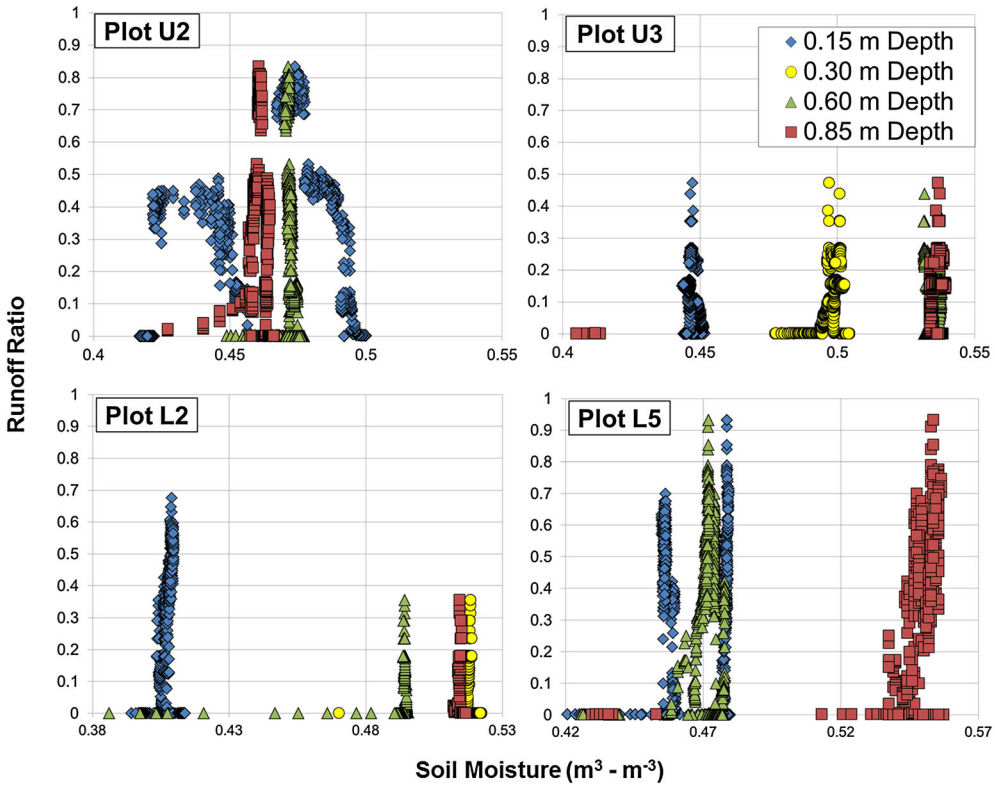

Figure 5. Volumetric soil moisture and run-off ratio for plots U2, U3, L2, and L5 during the 2012 (year 2) irrigation experiment

of their original surface area. Further crack closure then required greater increases in soil water content, with no real variation in soil water content observed during the final 20% of sealing. *Crackometer* U3-1 (also shown in Figure 7) had an opposite response, in that much of the 0.15-m depth soil water content increase occurred before the crack began to seal. This finding suggests that cracks may behave differently at the surface compared with the subsurface and that surface-based crack measurements may not be sufficient to predict subsurface crack behaviour.

Relative crack closure, as measured by both the surface crack imaging and the installed *crackometer* instruments, was compared with a run-off ratio (Figure 8). As with soil water content, the surface cracks showed a more uniform response than the responses measured by the *crackometer* instruments. In the case of the former, no run-off was observed until the surface cracks were more than 80% closed, and the run-off ratio increased as the surface cracks fully sealed. The *crackometer* measurements, however, showed run-off beginning when the cracks were only 60–70% closed and that the run-off ratio fluctuated with no corresponding variation in the apparent crack volume. However, both the surface imaging and the *crackometer* data showed a general trend of increasing run-off with decreasing crack size.

Contrary to most modelling approaches for *vertic* soils (and similar to the observational results of Wells *et al.* (2003)), these data suggest that run-off can occur before the cracks have fully sealed. The relationship appears to be consistent across plots and in response to different rainfall intensities. This result indicates that it may be possible to develop a simple modelling term to relate run-off to near-surface crack volumes.

Comparison of experimental treatments

The four experimental treatments showed that 0.23 m of rainfall gave rise to 0.01 to 0.05 m of cumulative run-off (Figure 9). Plots L1–L3 (the LT-HR treatment) and U4–U6 (the LT-LR treatment) showed very different responses from one another, suggesting that the intensity and duration of rainfall may affect the run-off threshold behaviour. Because the 0.23-m rainfall level of application was reached for most plots during the fifth irrigation, it is worthwhile to examine differences between treatments with regard to the fifth irrigation. Plots L1–L3 had a 1-week gap between irrigations 4 and 5, whereas plots U4–U6 received those same irrigations on consecutive days. Conversely, plots U1–U3 (the LT-MR treatment) received irrigations 4 and 5 with less than an hour between them yet produced less cumulative run-off than plots U4–U6. This difference suggests that time-dependent soil swelling effects

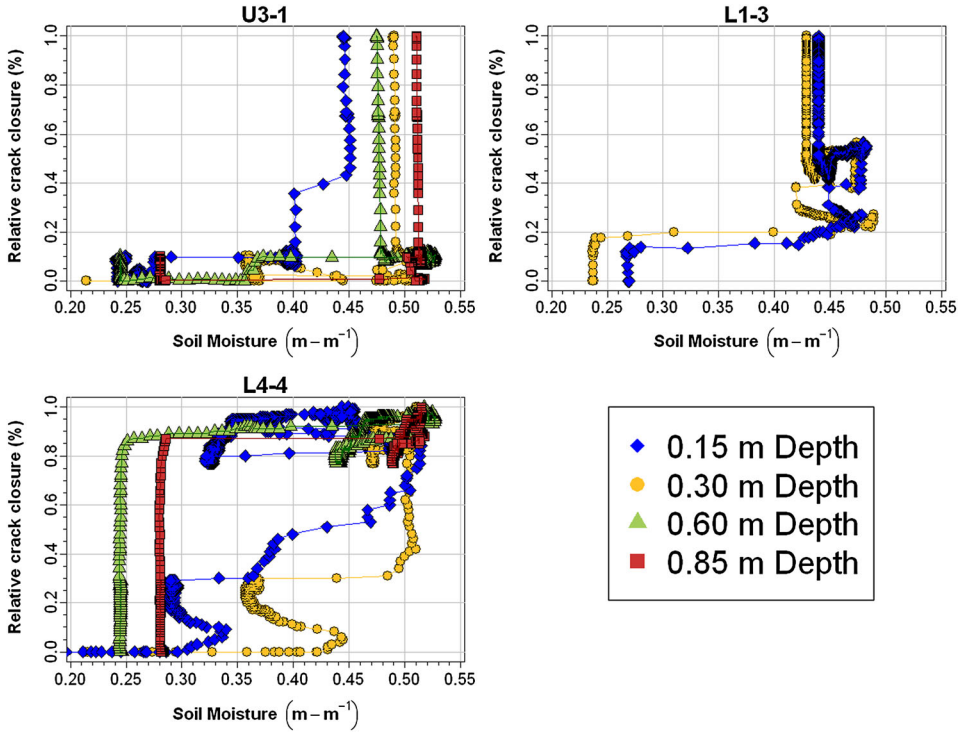

Figure 6. Volumetric soil moisture and the percent closure of representative cracks for plots U2, U3, L2, and L5 during the 2012 (year 2) irrigation experiment

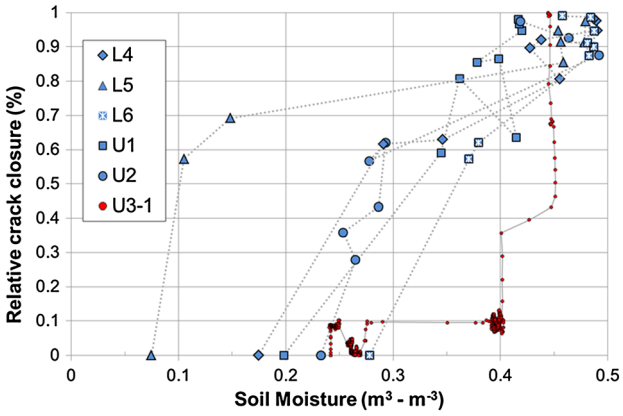

Figure 7. Crack closure *versus* soil moisture, where relative crack closure is estimated using the surface-based crack imaging (red). Crackometer data from plot U3 is also shown for comparison (blue). Soil moisture measurements come from the 0.15-m depth

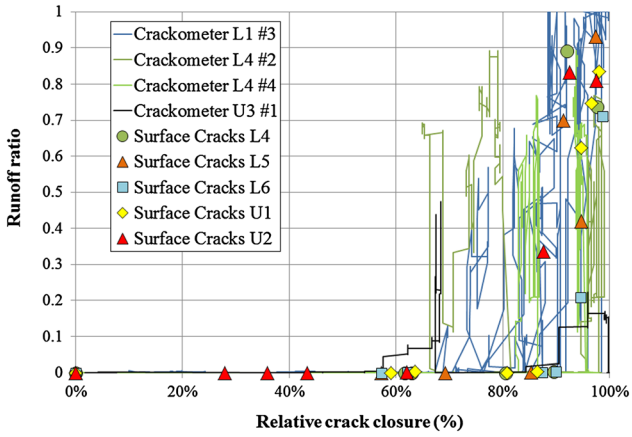

Figure 8. Run-off ratio compared with relative crack closure from both the surface imaging of selected cracks (points) and from the installed crackometer instruments (lines)

may be most pronounced on a timescale of around 1 day: At early times, the soil is still swelling, while at times longer than 1 day, water redistribution may become important. The crack swelling and soil water content data seem to support this conclusion, as both were seen to vary during the inter-irrigation periods (Figure 10). However, because of a limited number of replicates and high irrigation variability, no statistically significant differences in cumulative run-off were observed using the Student's *t*-test (p-value > 0.09). A greater number of replicates and better irrigation uniformity would be needed to truly assess any time-dependent or rate-dependent swelling impacts on run-off generation.

Cumulative rainfall and run-off

When the cumulative amounts of per plot simulated rainfall were plotted (based on 2012 data), an interesting trend emerged (Figure 11). No run-off was observed during the first 0.12 m of rainfall. Thereafter, in the narrow band

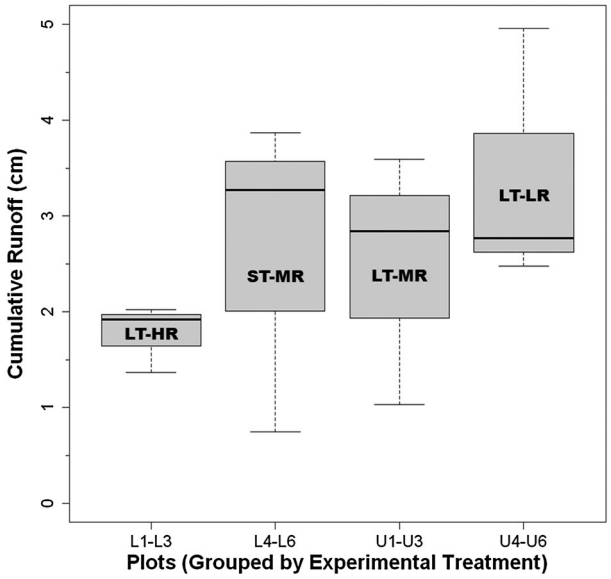

Figure 9. Difference in mean group run-off for the four experimental treatments: long-time, high-rate (LTHR); short-time, mixed-rate (ST-MR); long-time, mixed-rate (LT-MR); and long-time, low-rate (LT-LR)

between 0.12 and 0.17 m of cumulative precipitation, all plots began to produce run-off. This result correlates well with the pedotransfer function proposed by Steenhuis *et al.* (2013) to predict cumulative run-off (Q) based on cumulative precipitation (P) for saturated excess run-off:

$$Q = 0 \quad \text{for } P \leq T \tag{6}$$

$$Q = F(P - T) \quad \text{for } P > T \tag{7}$$

where F is the fraction of watershed contributing to run-off, and T is a threshold value related to the amount of available soil water storage.

Once the threshold value was reached and run-off began, there was a transition period in which the run-off response varied between plots. As discussed in the previous section, time between irrigation events could be a factor affecting how much run-off is produced. However, this effect may be transient, as after a transition period (of 0.05–0.1 m of additional rainfall), most of the plots again showed a similar run-off response. This finding agrees with previous observations that hydrological

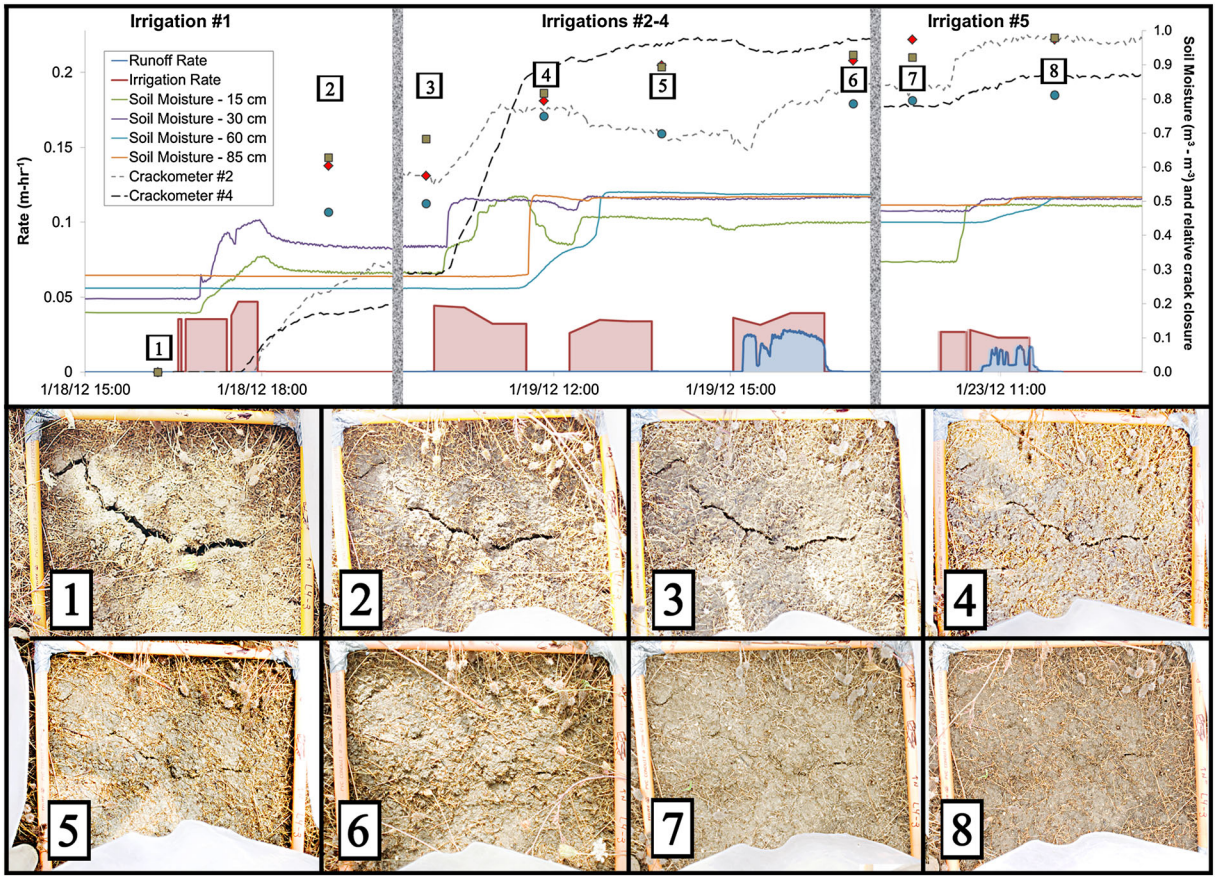

Figure 10. Time series for plot L4 during 2012 (year 2) experiment. Simulated rainfall (irrigation) and run-off are presented as rates, in red and blue, respectively. Soil moisture at 0.15 (green), 0.30 (purple), 0.60 (blue), and 0.85 m (orange) depths is shown as temperature-corrected volumetric data. Relative crack closure, taken to be $(V_{max}–V_i)/(V_{max}–V_{min})$, where V_i is the instantaneous measured volume, is shown as dashed lines for the crackometer data and as the discrete points for the crack imaging measurements. The images at bottom correspond to the green squares in the upper figure.

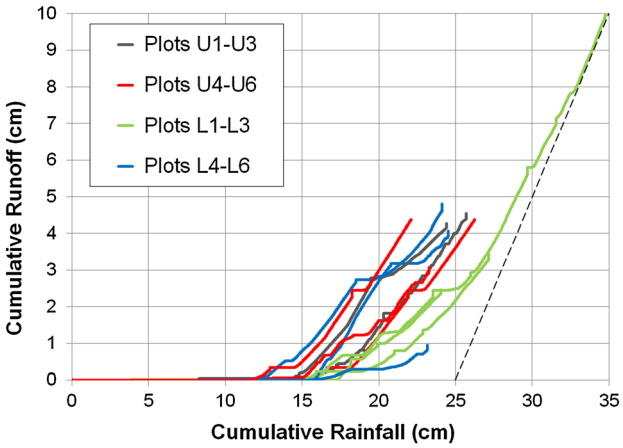

Figure 11. Cumulative amounts of rainfall (irrigation) and run-off for all plots during the 2012 (year 2) irrigation experiment.The 1:1 line is shown in black, starting at 25 cm of cumulative rainfall

predictability is the poorest in the vicinity of a nonlinear threshold and improves as the system moves away from that threshold (Blöschl and Zehe, 2005).

Finally, plot L1 received more rainfall than the others, and its run-off ratio approached unity (full run-off) after a cumulative rainfall amount of 0.33 m. This result suggests the possibility of a second run-off asymptote, when the subsurface pathways have become fully sealed, and can be seen when plotting run-off ratio as a function of cumulative rainfall (Figure 12). A rainfall amount of 0.33 m represents approximately one half of the area's mean annual rainfall, so it seems probable that this secondary level will be reached on occasion.

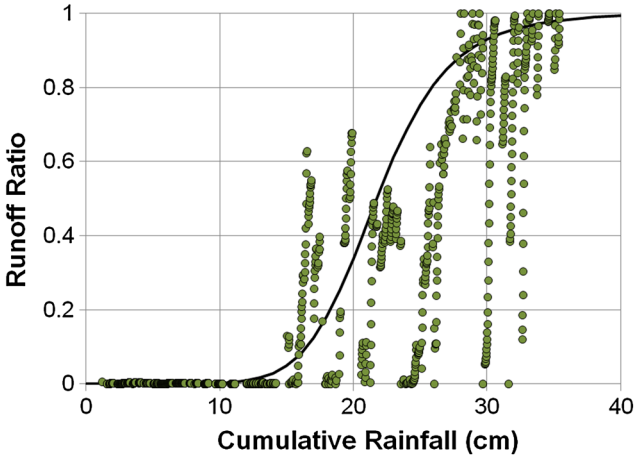

Figure 12. Run-off ratio as a function of cumulative rainfall for plot L1. The black line represents a sigmoidal function that potentially describes the transition between no run-off (run-off ratio = 0) and full run-off (run-off ratio = 1)

Infiltration results

The single-ring infiltration measurements had the largest variability and the highest mean value for effective hydraulic conductivity (K_{eff}), likely as a result of each measurement's small sample area (Table IV). The double-ring infiltrometer estimated K_{eff} values that were lower by one order of magnitude. The Guelph Permeameter had one measurement directly affected by a concealed crack, so its arithmetic mean for K_{eff} was higher than its geometric mean. The Mini-disk Tension Permeameter had consistent measurements that were 1–2 orders of magnitude smaller than the other surface-based tests, likely as a result of limited flow through macropores and cracks under tension. Altogether, these observations confirm the strong influence that near-surface cracks and macropores have on the K_{eff} of a dry *vertic* soil.

The single-ring infiltration measurements were used to plot near-surface K_{eff} as a function of initial degree of saturation for plots L2, L5, U2, and U5 (Figure 13). The coloured points in Figure 13 were calculated based on the arithmetic mean, which was considered to better represent the influence of small cracks on vertical flow (Stewart, 2013).

As the soil wetted, the near-surface effective hydraulic conductivity decreased to values of the same order of magnitude as the irrigation rate (0.02–0.05 m hr^{-1}). Further, the Guelph Permeameter data indicated that hydraulic conductivity of the soil decreases with depth. Thus, the observed run-off may have been caused by a combination of the decreased infiltration capacity of the soil, increased moisture content of the soil profile, and surface sealing of cracks.

Geophysical monitoring

It was observed that the apparent electrical conductivity (σ) of the soil downslope of the irrigation plots increased with time, corresponding to the periods of irrigation (Figure 14).

In the first monitoring event, no surface run-off was generated during the first two irrigations (Figure 14a), as all water infiltrated into the soil matrix. Interestingly, increases in the monitoring array apparent conductivity were observed during the first and second irrigations, long before any surface run-off occurred. This finding suggests that crack networks can move water laterally through the shallow subsurface, acting as the 'concealed surface run-off' pathways predicted by Horton over 70 years ago (Beven and Germann, 1982). Furthermore, the conductivity readings stayed relatively constant between irrigation events, suggesting that water remained stored within the crack network, satisfying its storage capacity and acting as a water source so that swelling and redistribution could occur.

Table IV. Summary of infiltration measurements taken over the 2-year experimental period

Method	K_{eff} (m hr^{-1})					
	No. of tests	Minimum	Maximum	Arithmetic mean	Geometric mean	Standard deviation
SRI[a]	62	1.58×10^{-2}	1.29×10^{1}	2.08×10^{0}	9.48×10^{-1}	2.92×10^{0}
DRI[b]	5	4.64×10^{-2}	5.41×10^{-1}	1.79×10^{-1}	1.17×10^{-1}	1.84×10^{-1}
GP[c]	6	1.20×10^{-4}	6.91×10^{-1}	1.16×10^{-1}	1.07×10^{-3}	2.57×10^{-1}
MTP	4	5.14×10^{-3}	1.32×10^{-1}	5.58×10^{-2}	2.55×10^{-2}	5.28×10^{-2}

SRI = single-ring infiltrometer, DRI = double-ring infiltrometer, GP = Guelph Permeameter, and MTP = Mini-disk Tension Permeameter.
[a] Only measurements with $\Theta_0 < 0.3$ were included for the SRI.
[b] An additional DRI test was attempted but emptied so rapidly that accurate data could not be collected.
[c] GP data are based on the minimum calculated K_{eff}, which assumes initially unsaturated soil and maximum matric potential.

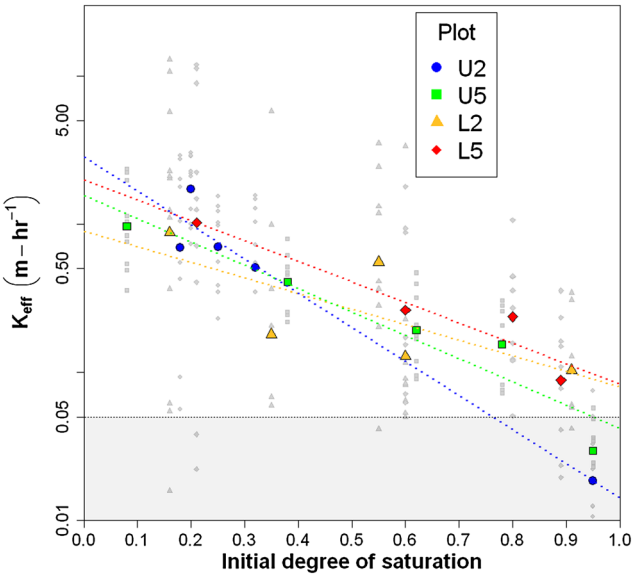

Figure 13. Effective hydraulic conductivity (K_{eff}) as a function of initial degree of saturation. The gray points represent individual measurements, while the coloured points represent the arithmetic mean of those measurements. The range of irrigation rates applied during the irrigation experiments are shown in the shaded box

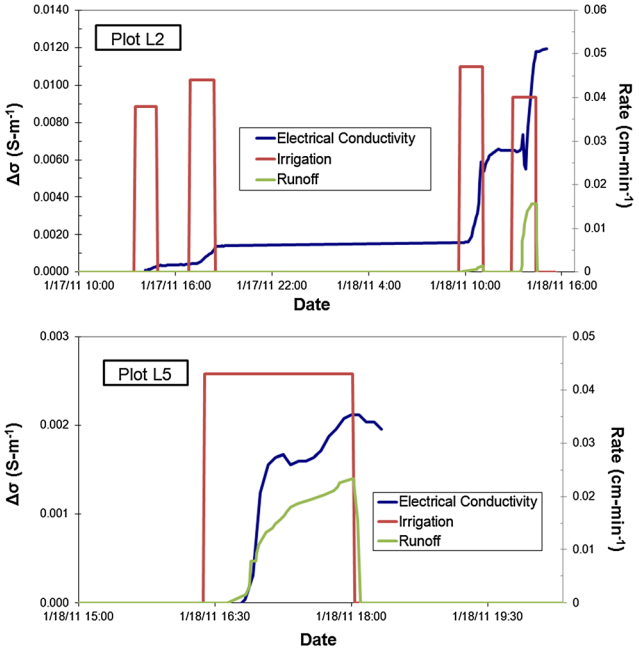

Figure 14. Change in apparent electrical conductivity for (a) plot L2 and (b) plot L5, along with the duration and amount of irrigation and run-off

After leaving the soil plots uncovered overnight, irrigation was resumed the next morning (the third irrigation event). The soil conductivity began to increase approximately 20 min after irrigation began, and 40 min later, surface run-off was measured leaving the plot. The soil apparent conductivity changed by a larger magnitude during the third irrigation as compared with the previous two irrigations. This may be explained by clay swelling processes decreasing the crack network void volume and sealing of some small transverse leakage paths. Under these conditions, a smaller volume of irrigation water would fill the crack network to a larger extent, thus inducing a greater change of apparent conductivity with the onset of irrigation and surface flow. Furthermore, the soil beneath the irrigation plot was near field capacity, meaning that water loss from the cracks through infiltration and diffusion would be minimal, and water could move downhill through the cracks under gravity.

During the fourth irrigation event, water was noted flowing out of cracks in the excavated pit that contains the collection barrel system. This visual observation confirmed the presence of lateral preferential flow and supported the interpretation of increases in electrical resistivity as being indicative of active lateral preferential flow paths. In contrast to lysimeter-scale study of Greve *et al.* (2012), in which surface ponding was judged to occur at the point of transition from preferential to matrix flow, these field-scale results show that subsurface preferential flow can still be active under ponded conditions.

In the second monitoring event, where the soil within the irrigation plot was already near field capacity, an increase in apparent electrical conductivity was observed at

approximately the same time as surface run-off began in the plot (Figure 14b). Immediately thereafter, subsurface seepage flow was observed emerging from the walls of the barrel collection box.

Taken together, these two monitoring events show that a flow through lateral surface or 'concealed run-off' pathways is an important hydrological process in both dry and wet conditions. In wet soils, their presence serves as further repudiation to the paradigm that cracks seal from the bottom up and that infiltration effectively ends when the soil surface is sealed. However, the dry soil response may be even more important. The ERT data indicated that water began moving laterally through the dry soil immediately after the start of the first irrigation, as evidenced by a resistivity decrease seen 2 m downhill within the first 45 min of the experiment. This flow in dry, unsaturated conditions may provide a point of distinction from lateral subsurface run-off seen in non-swelling soils; as in the latter, either local water tables must be developed (McGlynn *et al*., 2002; Tromp van Meerveld and McDonnell, 2005) or a threshold amount of precipitation and moisture must be reached (McGuire and McDonnell, 2010) for subsurface flow to occur.

One major drawback to the Wenner configuration used for these ERT measurements is that it does not provide for quantification of the amount of water being delivered preferentially. Therefore, it is hoped that future research will be directed towards better quantification and understanding of how water moves through subsurface crack flow paths.

SUMMARY AND CONCLUSIONS

A study performed on a set of 12 instrumented field plots demonstrated that, in a *vertic* soil, crack networks act as a dominant control on water movement. As seen in the previous studies, shrinkage cracks cause surface water to reach depths faster than would be expected from infiltration through the soil matrix.

Measurements made on representative cracks indicated that swelling of soil may proceed in phases. At the surface, the cracks initially showed rapid swelling, closing by more than 50% with little increase in the soil water content of the profile. From there, however, swelling proceeded slowly, and the near-surface soil reached field capacity before the cracks completely sealed. Subsurface-monitored cracks showed an opposite behaviour, in that the volume changed very little initially as the soil profile wetted, but as the moisture levels approached field capacity swelling proceeded rapidly. This result may substantiate the findings of Favre *et al*. (1997), who, using surface-based measurements, observed that soil at the crack interface showed more rapid and extensive swelling than the soil within the peds.

The relationship between run-off and soil water content (as measured by small capacitance sensors embedded at four depths into the soil peds) was nearly binary, where no run-off occurred until the soil water content reached a certain level, and then the soil water content showed very little change even with increasing run-off ratio. This effect may be an artefact of the capacitance sensors' limited sampling volumes, which may have constrained their ability to capture soil water content changes occurring at the ped-crack interface.

Infiltration data collected during the experiment indicated that in dry conditions, the soil matrix had a much higher infiltration capacity than would be predicted based on the soil texture, likely as a result of the presence of microscopic cracks. At high moisture contents, when the cracks had mostly sealed at the surface and the matrix infiltration capacity had decreased, water was still able to infiltrate at high rates. This was shown both by the run-off ratio, which for most plots peaked between 0.5 and 0.9 (indicating that 10–50% of the water being applied was still infiltrating), and by direct current resistivity measurements, which revealed the presence of active subsurface flow paths coincident with surface run-off. However, data collected from one of the run-off plots showed that the run-off ratio approached unity when additional water was applied. This hints at the existence of a secondary run-off asymptote in which the subsurface flow paths have become sealed.

Finally, it was found that using a basic water budget (cumulative precipitation minus evaporation) was an effective predictor of the primary run-off threshold. Indeed, it seems possible that this simple metric serves to integrate many of the complex processes observed in this study and allows us to conceptualize a *vertic* soil profile as a leaking bucket, only one in which the leak becomes smaller and possibly sealed through time. This simple concept may be useful to inform the development of more refined models that quantitatively describe the hydrology of a *vertic* soil.

ACKNOWLEDGEMENTS

This work was supported by National Science Foundation Grant No. 0943682. The authors wish to thank Sra. Irene Acevedo for generously providing the use of her property for purposes of this study. Likewise, the authors would like to recognize the contributions of Dr Diego Rivera, Mr Carlos Cea, Alejandra Lavados Carrasco, Abraham Arevalo Neira, and Viviana Gavilan Pino of the Department of Recursos Hídricos at the Universidad de Concepción, Chillán; Dr J. Reed Glassman of Willamette Geological Service; Brian Dougherty and John Hesseltine of Oregon State University; and Emeline Perret and Lifang Xie of

INP-ENSEEIHT. Any use of trade, firm, or product names is for descriptive purposes only and does not imply endorsement by the US Government.

REFERENCES

Abou Najm MR, Jabro JD, Iversen WM, Mohtar RH, Evans RG. 2010. New method for the characterization of three-dimensional preferential flow paths in the field. *Water Resources Research* **46**. DOI: 10.1029/2009wr008594.

Ahmad N. 1996. Occurrence and distribution of Vertisols. *Developments in Soil Science* **24**: 1–41.

Ali G, Oswald CJ, Spence C, Cammeraat EL, McGuire KJ, Meixner T, Reaney SM. 2013. Towards a unified threshold-based hydrological theory: necessary components and recurring challenges. *Hydrological Processes* **27**: 313–318.

Amidu SA, Dunbar JA. 2007. Geoelectric studies of seasonal wetting and drying of a Texas vertisol. *Vadose Zone Journal* **6**: 511. DOI: 10.2136/vzj2007.0005.

Arnold JG, Potter KN, King KW, Allen PM. 2005. Estimation of soil cracking and the effect on surface runoff in a Texas Blackland Prairie watershed. *Hydrological Processes* **19**: 589–603. DOI: 10.1002/hyp.5609.

Beven K, Germann P. 1982. Macropores and water flow in soils. *Water Resources Research* **18**: 1311–1325.

Blake G, Schlichting E, Zimmermann U. 1973. Water recharge in a soil with shrinkage cracks. *Soil Science Society of America Journal* **37**: 669–672.

Blöschl G, Zehe E. 2005. On hydrological predictability. *Hydrological Processes* **19**: 3923–3929.

Boivin P, Garnier P, Vauclin M. 2006. Modeling the soil shrinkage and water retention curves with the same equations. *Soil Science Society of America Journal* **70**: 1082. DOI: 10.2136/sssaj2005.0218.

Bouma J, Dekker LW. 1978. A case study on infiltration into dry clay soil I. Morphological observations. *Geoderma* **20**: 27–40.

Bouma J, Loveday J. 1988. Characterizing soil water regimes in swelling clay soils. In: *Vertisols: Their Distribution; Properties; Classification and Management*. Wilding LP, Puentes R (eds.) Texas A&M University Printing Center: College Station, TX; 83–96.

Brocca L, Melone F, Moramarco T. 2008. On the estimation of antecedent wetness conditions in rainfall–runoff modelling. *Hydrological Processes*, **22**: 629–642. DOI: 10.1002/hyp.6629.

Bronswijk J, Hamminga W, Oostindie K. 1995. Field-scale solute transport in a heavy clay soil. *Water Resources Research* **31**: 517–526.

Buringh P. 1989. Availability of agricultural land for crop and livestock. Food and natural resources: 69.

Campbell CS. 2001. Response of ECH2O soil moisture sensor to temperature variation. Decagon Devices Inc. Application Note AN70TP-10. Decagon Devices Inc., Pullman, Wash.

Chen L, Young MH. 2006. Green-Ampt infiltration model for sloping surfaces. *Water Resources Research* **42**. DOI: 10.1029/2005wr004468.

Chertkov VY. 2002. Modelling cracking stages of saturated soils as they dry and shrink. *European Journal of Soil Science* **53**: 105–118.

Chertkov VY. 2012. Physical modeling of the soil swelling curve vs. the shrinkage curve. *Advances in Water Resources*.

Dinka TM, Lascano RJ. 2012. Review paper: challenges and limitations in studying the shrink-swell and crack dynamics of vertisol soils. *Open Journal of Soil Science* **2**: 82–90.

Driessen P, Deckers J, Spaargaren O, Nachtergaele F. 2000. Lecture notes on the major soils of the world. Food and Agriculture Organization (FAO).

Evett SR, Schwartz RC, Tolk JA, Howell TA. 2009. Soil profile water content determination: Spatiotemporal variability of electromagnetic and neutron probe sensors in access tubes. *Vadose Zone Journal* **8**: 926–941.

Favre F, Boivin P, Wopereis M. 1997. Water movement and soil swelling in a dry, cracked Vertisol. *Geoderma* **78**: 113–123.

Giráldez JV, Sposito G, Delgado C. 1983. A general soil volume change equation: I. The two-parameter model. *Soil Science Society of America Journal* **47**: 419–422.

Goodrich D, Schmugge T, Jackson T, Unkrich C, Keefer T, Parry R, Bach L, Amer S. 1994. Runoff simulation sensitivity to remotely sensed initial soil water content. *Water Resources Research* **30**: 1393–1405.

Greco R. 2002. Preferential flow in macroporous swelling soil with internal catchment: model development and applications. *Journal of Hydrology* **269**: 150–168.

Greve AK, Andersen MS, Acworth RI. 2010. Investigations of soil cracking and preferential flow in a weighing lysimeter filled with cracking clay soil. *Journal of Hydrology* **393**: 105–113. DOI: 10.1016/j.jhydrol.2010.03.007.

Greve AK, Andersen MS, Acworth RI. 2012. Monitoring the transition from preferential to matrix flow in cracking clay soil through changes in electrical anisotropy. *Geoderma* **179-180**: 46–52. DOI: 10.1016/j.geoderma.2012.02.003.

Heppell C, Burt T, Williams R. 2000. Variations in the hydrology of an underdrained clay hillslope. *Journal of Hydrology* **227**: 236–256.

Hoogmoed W, Bouma J. 1980. A simulation model for predicting infiltration into cracked clay soil. *Soil Science Society of America Journal* **44**: 458–461.

James A, Roulet N. 2009. Antecedent moisture conditions and catchment morphology as controls on spatial patterns of runoff generation in small forest catchments. *Journal of Hydrology* **377**: 351–366.

Jarvis NJ. 1991. MACRO-A model of water movement and solute transport in macroporous soils. Reports and Dissertations No. 9. In: Department of Soil Sciences, Swedish University of Agricultural Sciences.

Jarvis NJ, Leeds-Harrison PB. 1987. Modelling water movement in drained clay soil. I. Description of the model, sample output and sensitivity analysis. *Journal of Soil Science* **38**: 487–498.

Kutílek M. 1996. Water relations and water management of vertisols. *Developments in Soil Science* **24**: 201–230.

McGarry D, Malafant KWJ. 1987. The analysis of volume change in unconfined units of soil. *Soil Science Society of America Journal* **51**: 290–297.

McGlynn BL, McDonnel JJ, Brammer DD. 2002. A review of the evolving perceptual model of hillslope flowpaths at the Maimai catchments, New Zealand. *Journal of Hydrology* **257**: 1–26.

McGuire KJ, McDonnell JJ. 2010. Hydrological connectivity of hillslopes and streams: Characteristic time scales and nonlinearities. *Water Resources Research* **46**: W10543.

Messing I, Jarvis NJ. 1990. Seasonal variation in field-saturated hydraulic conductivity in two swelling clay soils in Sweden. *Journal of Soil Science* **41**: 229–237.

Morari F, Knisel W. 1997. Modifications of the GLEAMS model for crack flow. *Transactions of ASAE* **40**: 1337–1348.

Morbidelli R, Corradini C, Saltalippi C, Brocca L. 2012. Initial Soil Water Content as Input to Field-Scale Infiltration and Surface Runoff Models. *Water Resources Manage* **26**: 1793–1807.

Návar J, Mendez J, Bryan RB, Kuhn NJ. 2002. The contribution of shrinkage cracks to bypass flow during simulated and natural rainfall experiments in northeastern Mexico. *Canadian Journal of Soil Science* **82**: 65–74.

Novák V, Šimůnek J, Van Genuchten MT. 2002. Infiltration into a swelling, cracked clay soil. *Journal of Hydrology and Hydromechanics* **50**: 3–19.

Peng X, Horn R. 2007. Anisotropic shrinkage and swelling of some organic and inorganic soils. *European Journal of Soil Science* **58**: 98–107.

Penna D, Tromp-van Meerveld HJ, Gobbi A, Borga M, Dalla Fontana G. 2011. The influence of soil moisture on threshold runoff generation processes in an alpine headwater catchment. *Hydrology and Earth System Sciences* **15**: 689–702. DOI: 10.5194/hess-15-689-2011.

Philip JR. 1957. The theory of infiltration: 4. Sorptivity and algebraic infiltration equations. *Soil Science* **84**: 257.

Ringrose-Voase A, Sanidad W. 1996. A method for measuring the development of surface cracks in soils: application to crack development after lowland rice. *Geoderma* **71**: 245–261.

Römkens MJM, Prasad SN. 2006. Rain Infiltration into swelling/shrinking/cracking soils. *Agricultural Water Management* **86**: 196–205. DOI: 10.1016/j.agwat.2006.07.012.

Samouëlian A, Cousin I, Richard G, Tabbagh A, Bruand A. 2003. Electrical resistivity imaging for detecting soil cracking at the centimetric scale. *Soil Science Society of America Journal* **67**: 1319–1326.

Samouëlian A, Richard G, Cousin I, Guerin R, Bruand A, Tabbagh A. 2004. Three-dimensional crack monitoring by electrical resistivity measurement. *European Journal of Soil Science* **55**: 751–762. DOI: 10.1111/j.1365-2389.2004.00632.x.

Sanders EC, Abou Najm MR, Mohtar RH, Kladivko E, Schulze D. 2012. Field method for separating the contribution of surface-connected preferential flow pathways from flow through the soil matrix. *Water Resources Research* **48**: W04534.

Selker JS, Keller CK, McCord JT. 1999. Vadose zone processes. Lewis Publishers.

Sentenac P, Zielinski M. 2009. Clay fine fissuring monitoring using miniature geo-electrical resistivity arrays. *Environmental Earth Sciences* **59**: 205–214. DOI: 10.1007/s12665-009-0017-5.

Smith R, Goodrich D. 2000. Model for rainfall excess patterns on randomly heterogeneous areas. *Journal of Hydrologic Engineering* **5**: 355–362.

Steenhuis TS, Hrnčíř M, Poteau D, Romero Luna EJ, Tilahun SA, Caballero LA, Guzman CD, Stoof CR, Šanda M, Yitaferu B, Císlerová M. 2013. A Saturated Excess Runoff Pedotransfer Function for Vegetated Watersheds. *Vadose Zone Journal* **12**. DOI: 10.2136/vzj2013.03.0060.

Stewart RD. 2013. Characterization of Hydrologic Parameters and Processes in Shrink-swell Clay Soils. In: Graduate School, Oregon State University, 207.

Stewart RD, Abou Najm MR, Rupp DE, Selker JS. 2012. Measurement Tool for Dynamics of Soil Cracks. *Vadose Zone Journal* **11**(2): vzj2011.0048.

Tariq A-u-R, Durnford DS. 1993. Analytical volume change model for swelling clay soils. *Soil Science Society of America Journal* **57**: 1183–1187.

te Brake B, van der Ploeg M, de Rooij G. 2012. Water storage change estimation from in situ shrinkage measurements of clay soils. *Hydrology and Earth System Sciences Discussions* **9**: 13117–13154.

Tromp van Meerveld I, McDonnell JJ. 2005. Comment to "Spatial correlation of soil moisture in small catchments and its relationship to dominant spatial hydrological processes, Journal of Hydrology 286: 113 134''. *Journal of Hydrology* **303**: 307–312.

van Dam JC. 2000. Simulation of field-scale water flow and bromide transport in a cracked clay soil. *Hydrological Processes* **14**: 1101–1117.

Verbist K, Cornelis W, Torfs S, Gabriels D. 2013. Comparing methods to determine hydraulic conductivities on stony soils. *Soil Science Society of America Journal* **77**: 25–42.

Vogel HJ, Hoffmann H, Leopold A, Roth K. 2005. Studies of crack dynamics in clay soil II. A physically based model for crack formation. *Geoderma* **125**: 213–223. DOI: 10.1016/j.geoderma.2004.07.008.

Warrick AW. 1983. Interrelationships of irrigation uniformity terms. *Journal of Irrigation and Drainage Engineering-ASCE* **109**: 317–332.

Weisbrod N, Dragila MI, Nachshon U, Pillersdorf M. 2009. Falling through the cracks: The role of fractures in Earth-atmosphere gas exchange. *Geophysical Research Letters* **36**: L02401.

Wells R, DiCarlo D, Steenhuis T, Parlange J-Y, Römkens M, Prasad S. 2003. Infiltration and surface geometry features of a swelling soil following successive simulated rainstorms. *Soil Science Society of America Journal* **67**: 1344–1351.

Zehe E, Elsenbeer H, Lindenmaier F, Schulz K, Blöschl G. 2007. Patterns of predictability in hydrological threshold systems. *Water Resources Research* **43**: W07434.

Zein el Abedine A, Robinson GH. 1971. A study on cracking in some vertisols of the Sudan. *Geoderma* **5**: 229–241.